Shear thickening in dense non-Brownian suspensions: Viscous to inertial transition

Y. Madraki, A. Oakley, A. Nguyen Le, A. Colin, G. Ovarlez, S. Hormozi

Shear thickening in dense non-Brownian suspensions: Viscous to inertial transition

Y. Madraki,[1] A. Oakley,[1] A. Nguyen Le,[2] A. Colin,[2,3] G. Ovarlez,[4] and S. Hormozi[1, a)]

[1)]*Department of Mechanical Engineering, Ohio University, Athens, Ohio 45701-2979, USA*

[2)]*ESPCI Paris, Sciences et Ingénierie de la Matière Molle, CNRS UMR 7615 10, PSL Research University, rue Vauquelin, F-75231 Paris Cedex 05, France.*

[3)]*Université de Bordeaux, Centre de Recherche Paul Pascal 115 avenue Schweitzer, 33600 Pessac, France.*

[4)]*University of Bordeaux, CNRS, Solvay, LOF, UMR 5258, 33608 Pessac, France*

(Dated: 30 January 2020)

We present an experimental study on the viscous to inertial mode of shear thickening in dense non-Brownian suspensions. We design a model suspension consisting of mono size spherical particles within a Newtonian suspending fluid. We develop a protocol for the rheological characterization of dense suspensions using the conventional rheometry technique. Our results provide constitutive laws for suspensions with solid volume fractions close to jamming when both viscous and inertial effects at the particle scale are present. We perform atomic force microscopy to measure forces between the particles immersed in the suspending fluid and show that our system of study corresponds to the frictionless regime of dense suspensions in which viscous and collisional forces dissipate the energy. Finally, we show that the proposed empirical constitutive laws, when approaching jamming, predicts the dynamics of dense suspensions in a transient boundary driven flow.

[a)]Electronic mail: Hormozi@ohio.edu.

I. INTRODUCTION

Suspensions of particles in a viscous liquid display a wide spectrum of non-Newtonian rheology including shear thickening, shear thinning, yield stress, and viscoelasticity[1–3]. Suspensions can be engineered to design smart materials that respond to external stimuli such as, pressure, light, vibration, electric field, temperature, and shear rate[4–7]. In shear thickening suspensions, viscosity appears to increase when the shear rate increases. These suspensions have many technological applications such as shock absorbing systems[8,9], protective clothings[10], flexible body armor[11], etc. Therefore, understanding the physics underlying the shear thickening phenomenon is of practical interest.

In non-Brownian suspensions, for which thermal fluctuations are negligible, different modes of shear thickening behavior have been identified. These modes are attributed to different physical mechanisms, which include: (i) hydrodynamic interactions between particles, (ii) transition from frictionless to frictional rheology, (iii) transition from viscous to inertial regime (Bagnoldian shear thickening[12]), and (iv) micro-structural effects. The third mode of shear thickening, i.e., Bagnoldaian shear thickening, is the focus of this work. We introduce a non-Brownian model suspension and provide the force measurements between the particles while immersed in the solvent. Also, we perform a comprehensive rheological study to show the transition from viscous to inertial shear thickening behavior in dense regimes. We show that our rheological constitutive law predicts the suspensions dynamics in a transient flow while the suspension transitions from viscous to inertial regime.

From this, we can now review existing literature on the shear thickening behavior in non-Brownian suspensions. In a shear thickening behavior, the rise in viscosity may happen in a continuous or discontinuous fashion leading to the Continuous Shear Thickening (CST) or Discontinuous Shear Thickening (DST) behaviors. In CST, a possible explanation for this behavior is the formation of hydro-clusters due to lubrication forces, the first mode of shear-thickening identified above[13,14]. Two approaching particles in a shear flow can be strongly coupled together under the action of lubrication hydrodynamics, which leads to the formation of these aforementioned hydro-clusters. The difficulty of particles flowing around one another and these hydro-clusters results in the extra rate of energy dissipation and consequently an increase in viscosity. In DST the apparent viscosity increases by several orders of magnitudes at a critical shear rate $\dot{\gamma}_c$. This framework comes short in explaining DST which occurs at a critical timescale.

A new promising way to understand CST and DST points to a transition from a frictionless to a frictional state of the suspension, the second mode of shear-thickening identified above[3,15–17]. The hypothesis is that there exists a short range repulsive force, F_R, among the grains preventing formation of a contact. This repulsive interaction will be overcome by hydrodynamic forces at large stresses or shear rates, i.e., $\dot{\gamma} \geq \dot{\gamma}_c$, converting the system into an assembly of frictional grains with a viscosity that diverges abruptly. The critical shear rate of transition is therefore $\dot{\gamma}_c = F_R/F_H$, where the denominator shows the typical hydrodynamic force. This hypothesis of friction-induced shear thickening is supported by recent experimental measurements[18–21] that validate the model and simulations. Particularly, in the recent work of Comtet et al.[21], a unique experimental procedure is developed, based on quartz-tuning fork atomic force microscopy, to directly measure inter-particle forces between particles in a suspending fluid.

For the third mode of shear-thickening, as we increase the shear rate, $\dot{\gamma}$, or solid volume fraction, ϕ[22,23], *inertia at the particle scale* becomes important and we transition from the viscous to inertial regime. In this third mode of shear thickening, the viscosity of the suspension increases linearly with the shear rate as proposed initially by Bagnold[12]. Several recent studies have focused on this inertial shear thickening, aiming to characterize the rheology of the suspensions (see[15,22–30]) as well as investigating the solid dispersion in flows with shear inhomogeneity[22,31].

Boyer et al.[32], have unified the rheology of dense suspensions to that of granular media. Therefore, a frictional view can be adopted to provide a better understanding of the key dimensionless numbers and the underlying physics when the viscous to inertial transition occurs in a non-Brownian suspension[27,33]. When an assembly of particles (with mean diameter d_p and density ρ_p) is suspended in a viscous fluid (with viscosity η_f and density ρ_f) and it is subjected to a steady shear under a confining particle pressure P, there is only one controlling dimensionless number associated with the shear rate. This shear rate can be interpreted as the ratio of the flow shear rate to the microscopic shear rate. Microscopic shear rate is defined by the time scale for particles to rearrange due to the pressure P.

Futhermore, the microscopic shear rate can be determined by writing the second law of Newton when the forces applied on a particle are the imposed pressure, P, and the drag force. In cases with negligible drag force, the rearrangement of particles is solely governed by the imposed pressure leading to the dimensionless number $I = \dot{\gamma} d_p/\sqrt{P/\rho_p}$. This is associated with the granular regime when momentum transport in the system is due to contacts and collisions among particles. When the imposed pressure balances the viscous drag force, the governing dimensionless number is

$J = \eta_f \dot{\gamma}/P$. This is associated with Stokesian suspensions when the viscous stresses are the main mechanism for the transport of momentum. Finally, when the turbulent drag at the particle scale balances P, the governing dimensionless number is $J_I = \rho_f (d_p \dot{\gamma})^2/P$ and the dynamics of the suspensions is governed by the inertia of the fluid phase.

In this work, our focus is on the viscous to inertial mode of shear thickening which corresponds to dense suspensions which transition from Stokesian (J dominated regime) to granular regime (I dominated regime). In the Stokesian regime stresses scale viscously while in the granular regime stresses scale inertially resulting in a viscosity proportional to the shear rate. Recently, there have been several numerical (via performing Discrete element method simulations) and theoretical works on this mode of shear thickening. On the macroscopic front, the closures for the shear stress and particle stress in terms of ϕ and $\dot{\gamma}$ are found. In terms of frictional view, it is equivalent of saying, the solid volume fraction and stress anisotropy, μ, are found as a function of I or J[25,28,34–36]. The transition from the viscous to inertial regime has been characterized to occur at the Stokes number, $St = I^2/J = \rho_p d_p^2 \dot{\gamma}/\eta_f$ of order of unity. On the microscopic front, the macroscopic quantities such as μ and ϕ are shown to depend on the microscopic quantities such as the relative velocity between particles, the strain scale beyond which a particle loses memory of its direction relative to its neighbors, the coordination network, the fraction of frictional contact, and the forces at the contact[16,23,25,37–42]. There exists a discrepancy among these works due to the assumption of different closures for inter-particle forces (friction and repulsive forces), type of weak contacts, the range of solid volume fraction explored, etc. For example, some numerical results show that a dense suspension transitions from viscous to inertial regime at $St \sim 1$[25,35], while others show that as we approach the jamming volume fraction, St of the transition strongly depends on the value of solid volume fraction[23,37–42]. The objective of this work is to explore experimentally the viscous to inertial transition in dense suspensions close to jamming while inter-particle forces are known via atomic force microscopy measurements.

The fourth mode of shear thickening corresponds to cases when weak hydrodynamic inertia at the particle scale affects the pair distribution function around a particle. Due to the presence of inertia, the Stokesian rheological measurements of non-Brownian suspensions are no longer valid, yet inertia of the fluid phase is not dominant and consequently J_I is not a relevant dimensionless number. For suspensions with particle Reynolds number of $Re_p = \rho_f d_p^2 \dot{\gamma}/\eta_f$, in the range $Re_p \in [.02, 10]$, and solid volume fraction ϕ, in the range $\phi \in [0.1, 0.4]$, the suspension viscosity increases as Re_p increases[43–47]. Due to the improvement of computational methods, see e.g.,[44,46,48–50],

interface resolved simulations of solid particles in Newtonian fluids can now reveal details of the suspension's micro-structure, and shed light on the role of inertia in the overall dynamics[51]. More precisely, the study of Picano et al.[45] shows that inertia affects the suspension's microstructure, resulting in an enhancement of effective shear viscosity. As Re_p increases, the average particle-pair relative motion in the suspension becomes increasingly anisotropic forming a wake region behind the particles with an almost zero probability of finding a second particle. These excluded volumes enhance the effective solid volume fraction as we increase the shear rate (or equivalently Re_p) and consequently the effective shear viscosity, leading to a shear-thickening behavior. This micro-structure effect has been shown to also be the case for non-Brownian suspensions with generalized Newtonian interstitial suspending fluids[47].

FIG. 1 summarizes the above studies that we explained in the plane of the solid volume fraction ϕ and particle Reynolds number $Re_p = \rho_f \dot{\gamma} d_p^2/\eta_f$ when dealing with the suspension of non-Brownian particles in a Newtonian viscous fluid. It is noteworthy to mention that we might have not included all the existing work due to the space limitation, and the main objective of presenting FIG. 1 is to show where our present study stands in terms of the ranges for ϕ and Re_p.

FIG. 1: The map of existing work. Due to the space limitation, the names of the leading authors of existing work are presented.

The main novel contributions of our study are as follows. Firstly, we introduce in detail the design of a model non-Brownian suspension that can be used in conventional volume imposed rheometry setups for investigating the physics of dense suspensions. The model suspension is composed of mono size spherical particles with the same density as the suspending fluid. Therefore, the rheology results exclude the effects of irregular shapes, polydispersity, and solid volume fraction inhomogeneities due to gravity (section II). Secondly, we develop a protocol for rheological characterization of dense suspensions using conventional rheometry setups. Our experimental method provides understanding about the distribution of velocity and solid volume fraction within the domain without using high-tech experimental tools such as magnetic resonance imaging[22], X-ray radiography, or computed tomography scan[52] (sections II, II A and Supplementary Material). Thirdly, we provide constitutive laws for the suspensions with solid volume fractions approaching jamming ($\phi < \phi_m \approx 0.605$) and we explain the underlying physical mechanisms for the transportation of momentum via providing atomic force microscopy measurements between the

particles immersed in the suspending fluid (section III). This comprehensive experimental study from a microscopic force measurements to a macroscopic rheological characterization provide benchmark data for the refinement and development of ongoing theoretical and computational research regarding viscous to inertial transition in dense suspensions[23,25,37–42]. Finally, we show that our proposed constitutive law predicts the dynamics of dense suspensions in a transient boundary driven flow when the transition from Stokesian to inertial regimes of suspensions occurs (section III D). We summarize the present work in section IV.

II. EXPERIMENTS

This section includes our experimental protocol. We encourage the experimental reader to see the Supplementary Material for steps that need to be taken into account to reproduce these results. The Supplementary Material includes the details of the sample preparation, the calibration of the vane tool geometry and instrument, inertial correction, and discussion on the critical Taylor number.

The model suspensions are made up of Polystyrene spherical particles (Microbead Dynoseeds, TS40 and TS80 with the company reported density of 1.05 g/cm^3) and an interstitial aqueous solution. Experiments are performed with two particle size ranges of $38-45\ \mu m$ and $75-90\ \mu m$ with the average particle diameter of $d_p = 41.5,\ 82.5\ \mu m$, respectively. The interstitial aqueous solution, mixture of Sodium Iodide (Sigma Aldrich, U.S.A.) and deionized water, was chosen to match the density of the particles. We added a small amount of Triton X-100 (laboratory grade, from Sigma Aldrich, U.S.A.) to remove the effect of polystyrene particles being hydrophobic.

We perform volume imposed rheometry tests on the suspension with a constant concentration, ϕ. We use vane tool geometry in a cup with an inner radius of $R_b = 14.0\ mm$, an outer radius of $R_c = 15.2\ mm$, a gap of $H = 1.2\ mm$, and a height of $L = 42\ mm$. Using a vane tool enables us to work with very dense suspensions. It eliminates the wall slip effect compared to the cup and bob geometry. Additionally, the vane and cup geometry requires a larger sample size compared to the parallel plates. This helps to ensure that we have a relatively insignificant evaporation over the duration of our experiment. We calibrate the vane tool via performing rheometry with cone and plate geometry.

The rheometry test that is chosen for these experiments is a stress imposed step or creep test. This involves imposing a constant stress for a set period of time. At the beginning of the experiments, for all imposed torques, we apply a pre-shear step, $T = 0.18\ \mu N.m$ for a short time ($strain < 500\%$). This ensures the suspension is in an anisotropic state at the beginning of the test[53]. In addition to this, we use fast sampling mode. This feature provides us with high frequency data acquisition rate at the start of the experiment and gradually decreasing rate as time passes. This is necessary due to the importance of having a sufficient amount of data points collected at the transient regime, which occurs at the beginning of the experiment.

A. A typical example of rheometry measurements

FIG. 2 shows a schematic and a typical output of our experimental method. We impose a constant stress on the vane tool after slight pre-shearing of the suspension. The applied pre-shear history ensures that the suspension is at the anisotropic state at the start of the rheometry test. As the constant stress is applied a transient boundary driven flow establishes itself with a Neumann boundary condition in terms of velocity at the inner boundary (or equivalently a constant local shear rate) and no-slip velocity at the outer boundary. While the radial derivative of the azimuthal velocity is imposed at the inner boundary, the velocity itself varies and diffuses across the gap until steady state is achieved. Therefore, the average shear rate increases as the velocity increases, see FIG. 2(a).

The output of the rheometer is the average shear rate and it is shown in FIG. 2(b). We explain more about measured shear rate in Supplementary Material. We can see that the average shear rate at the inner boundary increases with time or applied strain and reaches a plateau, signifying steady state, shown in FIG. 2(b). This steady state shear rate is associated with the stress imposed at the boundary. After some time, we observe a departure from the steady state plateau. Since the shear rate is not homogeneous across the gap, particles migrate from the inner boundary (the region of high shear rate) to the outer boundary (the region of low shear rate). This phenomenon is known as shear induced migration and the reader is referred to the following initial studies as well as more recent work[13,52,54]. We emphasize that the migration occurs very rapidly in dense suspensions[22]. A consequence for our experiments is that only a single measurement can be taken from a given

FIG. 2: (a): Schematic view of the stress imposed experiment and velocity evolution in the domain. (b): Three regimes of transient, steady state, and migration for the suspension of $\phi = 0.58$ and imposing constant torque of $T = 1.5\ \mu N.m$. The figure shows the average shear rate, $\bar{\dot{\gamma}}(s^{-1})$, versus time, $t(s)$.

sample. For any other creep test, a fresh sample has to be used.

A series of experiments have been carried out for a wide range of stress imposed on the prepared dense suspensions (described in section III A), with various solid volume fractions and two particle sizes of $d_p = 41.5$ and $82.5\ \mu m$. These experiments are performed with *Pe* number in the range of $3.66 \times 10^6 - 7.33 \times 10^8$. We have also checked that our measurements are reproducible within 5% error. The steady state shear rate associated with the applied stress is measured to provide constitutive laws for dense suspensions.

III. RESULTS

This section presents our results and provides constitutive laws close to jamming, section III A. We have carried out atomic force microscopy measurements to understand the physics underlying the proposed constitutive laws, sections III B and III C. We show the validity of the constitutive laws in predicting transient boundary driven flow of dense suspensions in settings where the transition from viscous to inertial regimes takes place, section

III D.

A. Constitutive law close to jamming

First, we start with presenting the relationship between the stress and shear rate in the dense suspensions used in the present work. FIG. 3 (a) & (b) show the plot of stress versus shear rate when performing experiments with particle size $d_p = 41.5\ \mu m$ and $d_p = 82.5\ \mu m$, respectively. The results indicate that, for all volume fractions and particle sizes, stress increases with the applied shear rate in a linear fashion, shown by filled circles that follow a solid line of slope 1 . However, after a critical shear rate, stress enhances quadratically with shear rate. It is shown by open circles which follow a dashed line of slope 2. Therefore, the suspensions transition from viscous to inertial regime at the critical shear rate denoted by $\dot{\gamma}_{v \to i}$, with the values reported in

TABLE I. It is evident that the shear rate of transition depends on both the solid volume fraction and the particle size.

We have plotted the data in terms of particle Reynolds number $Re_p = \rho_f d_p^2 \dot{\gamma}/\eta_f$ to better understand the onset of transition from viscous to inertial regime. FIG. 3 (c) & (d) show that the transition occurs at values of $Re_p << 1$, contradicting what has been shown numerically[25,55–58].

Here, we argue that, in our system of study focused on volume fractions close to jamming, the local particle Reynolds number is the relevant dimensionless number for the viscous to inertial transition. In dense suspensions, particularly close to jamming, the local shear rate $\dot{\gamma}_{local}$ in the interstitial fluid at the particle scale is much larger than the bulk shear rate, $\dot{\gamma}$, applied on the boundaries of suspensions. The local shear rate is the sole function of geometry and linked to $\dot{\gamma}$ as follows: $\dot{\gamma}_{local} = \mathscr{F}(\phi)\dot{\gamma}$. There exist both experimental and theoretical closures for the geometrical function $\mathscr{F}(\phi)$[23,59,60]. On the experimental front, $\mathscr{F}(\phi)$ is measured via a pressure imposed rheometer for dense non-Brownian suspensions[59]. The theoretical estimate of $\mathscr{F}(\phi)$ is given via the homogenization approach[60], as well as the perturbation method around the jammed state[23]. $\mathscr{F}(\phi)$ is a monotonically increasing function of ϕ and diverges at jamming volume fraction ϕ_m. Here, in our calculations, we used the following relations for obtaining $\mathscr{F}(\phi)$ which is experimentally obtained by Dagois-Bohy et al.,[59] with constants reported to be $\alpha = 4.6$, $\beta = 6$, $\kappa = 0.75$, $\mu_0 = 0.3$ and $\phi_m = 0.605$.

$$\mathscr{F}(\phi) = 2.8\sqrt{\eta_s(\phi)}$$

$$\eta_s = \mu(\phi)\eta_n(\phi)$$

$$\eta_n(\phi) = \kappa(\frac{\phi_m - \phi}{\phi})^{-2}$$

$$\mu(\phi) = \mu_0 + \alpha(\frac{\phi_m - \phi}{\phi}) + \beta(\frac{\phi_m - \phi}{\phi})^2$$

Therefore, the velocity scale at the particle scale is $\dot{\gamma}_{local} d_p$ and the relevant particle Reynolds number for which the transition occurs is $(Re_p)_{local} = \rho_f d_p^2 \dot{\gamma}_{local}/\eta_f$, which is larger than Re_p particularly as $\phi \to \phi_m$. This has been shown in FIG. 3 (e) & (f). This dependency of Reynolds of transition from viscous to inertial regime on the solid volume fraction is in line with the theoretical results of Wyart and co-workers[23,37,39–42], i.e., perturbation close to jamming. We will further discuss this matter in section III C.

FIG. 3: Presenting transition from viscous to inertial regime; (a)&(b): Stress, τ, Vs. shear rate for two particle sizes of $d_p = 41.5\ \mu m$ and $d_p = 82.5\ \mu m$, respectively. (c)&(d): Stress, τ, Vs. particles Reynolds number Re_p for two particle sizes of $d_p = 41.5\ \mu m$ and $d_p = 82.5\ \mu m$, respectively. (e)&(f): Stress, τ, Vs. local particles Reynolds number $(Re_p)_{local}$ for two particle sizes of $d_p = 41.5\ \mu m$ and $d_p = 82.5\ \mu m$, respectively. Solid lines are indicating slope 1. Dashed lines are indicating slope 2.

TABLE I: The transition shear rate from viscous to inertial regime, $\dot{\gamma}_{v\to i}$, shown for two particle diameters and for variation of particle concentration.

$d_p = 41.5\ \mu m$					
ϕ	0.56	0.57	0.58	0.59	0.595
$\dot{\gamma}_{v\to i}$	2.499	1.6	1.1		
$d_p = 82.5\ \mu m$					
ϕ	0.56	0.57	0.58	0.59	0.595
$\dot{\gamma}_{v\to i}$		3.21	2.21	0.82	0.31

It is noteworthy to mention that we have about 15 to 29 particles across the gap size of $H = 1.2\ mm$; therefore, the relationship between shear rate and stress does not depend on the gap size between the vane tool and the outer cylinder. We validated this point by obtaining a good agreement in comparison of our results with those reported by Fall et al.,[22] where the experiments were carried out in a wide-gap Couette geometry with a large gap size of 1.9 *cm*, see the Supplementary Material for more details about this comparison. We would like to mention that the scope and method of this work are different from that of Fall et al.,[22] in a sense that we merely enlighten on the viscous to inertial mode of shear thickening in dense non-Brownian suspensions (using conventional rheometry technique). We examine it for a range of solid volume fractions and different particle sizes. Additionally, we provide atomic force microscopy measurements (section III B) to show this mode of shear thickening is different from those caused by the significant role of frictional forces[3,15–17].

Here, we fit a curve to our data presented in FIG. 2 to provide the following relationship between the shear rate and shear stress at the dense regime.

$$\tau = (1-\mathscr{H}(\dot{\gamma}-\dot{\gamma}_{v\to i}))\eta_s(\phi)\eta_f\dot{\gamma}+\beta(\phi)\rho_p d_p^2\dot{\gamma}^2\mathscr{H}(\dot{\gamma}-\dot{\gamma}_{v\to i}). \quad (1)$$

The Heaviside step function is denoted by $\mathscr{H}$. In order to understand the physical origin of the terms in equation (1), we have performed atomic force microscopy to provide a measurement of inter-particle forces.

B. Atomic force microscopy

This section provides measurements of the dissipative forces (both of hydrodynamic and frictional origins) and repulsive forces of polystyrene spherical particles, of size $d_p = 140\ \mu m$, immersed in the suspending fluid used in this study.

FIG. 4: Force measurement using atomic force microscopy. (a): Tangential measured force, F_T Vs. distance, z. (b): Normal measured force, F_T Vs. distance. (c) Tangential measured force, F_T Vs. normal measured force, F_T.

The dissipative and repulsive forces of the suspension are measured via a unique experimental tool. The reader is referred to the work of Comtet et al.,[21] for a detailed description of the experimental tool and procedure. In summary, the interactions of two particles in a flow are measured by using tungsten tip glued to a millimeter quartz fork, a force sensor. Using a nano-manipulator integrated in a scanning electron microscope, a particle is attached to the end of this tip. This attached particle is immersed in a solvent and brought into contact with another particle on a silica wafer. To measure the force profiles between two approaching particles, the tuning fork is excited at two distinct resonance frequencies corresponding to the normal and shear modes of the quartz fork. The normal and tangential forces between the two approaching particles are measured via analyzing the variations of the resonance of each mode. The hydrodynamic and friction origin forces are distinguished by relaxation properties. In addition, repulsive forces are measured before the particles come into contact.

FIG. 4 shows the results of characterizing pairwise inter-particle interactions through the tangential friction force F_T (FIG. 4 a) and the normal dissipation force F_N (FIG. 4 b) versus distance

z, values where $z > 0$ correspond to the hydrodynamic lubrication regime and $z \leq 0$ correspond to the hard contact. We plot, in FIG. 4 c, the tangential dissipative force F_T versus the normal load F_N. Small values of F_N correspond to the regime of hydrodynamic lubrication. Data shows a line of slope almost zero indicating negligible friction coefficient in the hydrodynamic regime. As we exceed a critical normal load $F_N^C = 11.6 \pm 4\ \mu N$, the particles come into a hard contact and friction becomes important. This regime is well characterized by Amontons-Coulomb law, with a line of slope 0.0144 which shows the friction coefficient. It is noteworthy to mention that the value of the critical normal load $F_N^C = 11.6 \pm 4\ \mu N$ can also be seen in FIG. 4 b when $z = 0$. The atomic force microscopy measurements have been repeated 9 times. Moreover, the repulsive force is a surface force and, therefore, it is proportional to the particle size that is taken into account in our following calculations of stresses[61].

The critical value of stress at which the particles come into contact and transition from frictionless to frictional regime occurs at $\tau^C = C_\alpha F_N^C/(\pi(d_p^2/4))$. Where, C_α denotes a multiplier that relates the microscopic force measurements to the macroscopic stress values and it is of order of 0.01[3]. Therefore, the transition from a frictionless to a frictional system occurs at the stresses of order $20Pa$ and $10Pa$ for the particle sizes of $d_p = 41.5\ \mu m$ and $d_p = 82.5\ \mu m$ respectively. These values of stresses are well beyond the range of stress in our system of study (see FIG. 3). More precisely, our model suspensions transition from viscous to inertial regime at the stress of order $\tau_{v\to i} \sim 0.1\ Pa$, which is much less than the required stresses for the hard contact to occur. Therefore, our study explores viscous to inertial transition in a frictionless state of dense suspensions. Such a system shows DST or transitions to a frictional regime at much larger values of stress (i.e., larger than $20Pa$ and $10Pa$ for the particle sizes of $d_p = 41.5\ \mu m$ and $d_p = 82.5\ \mu m$ respectively). We refer the reader to the computational work of Ness and Sun[35], where three different systems with (1) $\tau^C \sim \tau_{v\to i}$; (2) $\tau^C > \tau_{v\to i}$ and (3) $\tau^C < \tau_{v\to i}$ have been studied. It is educative to see, from the work of Ness and Sun[35], how stresses vary with Stokes number in the aforementioned three systems. In system (2), which is the focus of our study, the critical Stokes number for the transition from viscous to inertial regime is not of the order of unity. We discuss this point in section III C.

C. Scaling argument

Here, we follow the work of Degiuli et al.,[23] and Bagnold[12] to provide scaling arguments for the form of constitutive laws of dense suspensions in both Stokesian and inertial regimes in the absence

of friction. The scaling argument of Degiuli et al.,[23] is based on the energy conservation while the scaling argument given by Bagnold[12] is based on the momentum exchange. Here, we explain both of the arguments and show they are similar. Moreover, we compare the predictions of these scalings to our experimental measurements and we disclose questions that should be answered via theoretical, computational, and experimental approaches to have a full understanding of the problem.

The conservation of energy imposes a strong constraint on the over-damped dynamics of dense suspensions with $\phi \to \phi_m$. We assume that the total power $\mathscr{P}^t = \Omega\tau\dot{\gamma}$ is injected to the system of volume Ω via imposed shear stress τ. This power dissipates within the system through viscous and collisional forces. The dissipation due to the viscous lubrication can be estimated as $\mathscr{P}^v \sim \eta_f N \delta V^2 d_p$, where η_f and N denote the viscosity and number of particles. Here, δV is the velocity scale at the particle scale and is given by $\mathscr{F}(\phi)\dot{\gamma}d_p$ (see section III A).

In inertial suspensions, a part of energy dissipates due to collisions among particles. Each time a particle changes its direction with respect to its neighbors, a finite fraction of its kinetic energy dissipates. This is proportional to $m_p\delta V^2 e$, where e is the coefficient of restitution and m_p is the mass of the particle. As we approach jamming $\phi \to \phi_m$, the time interval of a collision decreases. Moreover, the strain scale ε_c, at which velocities of particles decorrelate, approaches zero. Here, ε_c is the strain scale beyond which a particle loses memory of its direction relative to its neighbors and its estimate is given as $\varepsilon_c \sim \frac{1}{\mathscr{F}(\phi)^2}$,[23]. The power dissipated within the system due to collision is approximately $\mathscr{P}^s \sim N(\dot{\gamma}/\varepsilon_c)m_p\delta V^2$.

The total power injected in the system is equal to the dissipation of power through viscous and collisional effects as shown below

$$\mathscr{P}_t = \tau\dot{\gamma}\Omega = \mathscr{P}_v + \mathscr{P}_c = C_v\eta_f N\delta V^2 d_p + C_c N(\dot{\gamma}/\varepsilon_c)m_p\delta V^2. \tag{2}$$

Where C_v and C_c are constant multipliers and their values depend on the shape of particles.

There are several implications of equation (2). First, the scaling for the suspension stress can be obtained by dividing this equation by $\dot{\gamma}\Omega$ to have a constitutive law of the following form:

$$\tau = \eta_s(\phi)\eta_f\dot{\gamma} + \eta_I(\phi)\rho_p d_p^2\dot{\gamma}^2. \tag{3}$$

Our empirical constitutive law given in equation (1) can be written in the form similar to equation (3) which is in line with the conservation of energy. More specifically, the form of equation (1) was initially adopted to have the best curve fitting to our experimental measurements (mainly for

the modeling purposes that we explain in the next section). Second, we can balance the energy dissipation due to the viscous effects and collision effects to give an estimate for the shear rate of transition from the viscous to inertial regime as follows: $\dot{\gamma}_{v\to i} \sim \frac{\eta_f d_p}{m_p}\varepsilon_c \sim \frac{\eta_f}{\rho_p d_p^2}\frac{1}{\mathscr{F}(\phi)^2}$. This scaling shows that the shear rate of transition from the viscous to inertial regime approaches zero as we get close to the jamming volume fraction, i.e., $\dot{\gamma}_{v\to i} \to 0$ as $\phi \to \phi_m$. Therefore, the suspension transitions from the viscous to inertial regime at a very small particle Reynolds number or Stokes number as we approach jamming, which is consistent with our experimental measurements shown in FIG. 3 (c) & (d). Third, as a consequence when close to jamming, the relative shear viscosity, $\eta_s(\phi)$, and inertial viscosity, $\eta_I(\phi)$, are not identical. Therefore, the transition from the viscous to inertial regime occurs at a particle Reynolds number which depends on the value of the solid volume fraction and the transition does not necessarily occur at $Re_p \sim 1$.

Alternatively, the above scaling argument can be explained based on momentum exchange in the system. Here, we follow the explanation of Bagnold[12] and we show that the scaling argument based on momentum exchange results in the same conclusion as that of conservation of energy.

Bagnold assumed the following estimation for the local shear rate between grains of particles $\dot{\gamma}_{local} = \dot{\gamma} f'(\lambda)$. Where, λ is the linear grain concentration and it is defined as $\lambda = d_p/(d_{sep} - d_p) \sim \left[(\phi_m/\phi)^{1/3} - 1\right]^{-1}$, where d_{sep} is the center to center distance between the particles. In the collision dominated regime of suspensions during a collision, a particle experiences a total change of momentum of the order of $m_p \dot{\gamma} d_p$. An estimate for the number of collisions was assumed by Bagnold to be of the order of $f(\lambda)\dot{\gamma} d_p/S$, where S denotes the surface to surface distance between the particles. Therefore, the scaling for the stress in the collision dominated regime is $\frac{1}{d_{sep}^2}\frac{f(\lambda)\dot{\gamma} d_p}{S} m_p \dot{\gamma} d_p$. In the viscous dominated regime, the scaling for the stress is of the order of $\frac{\dot{\gamma} d_p \eta}{S} f'(\lambda)$. The main assumption of Bagnold is as follows $f(\lambda) = f'(\lambda) = \lambda$. Therefore, we can balance the exchange of of the momentum in the collision dominated regime and in the viscous dominated regime and show that $\dot{\gamma}_{v\to i} \sim \frac{\eta d_p}{m_p}\frac{1}{\lambda^2}$. Similarly, following the energy argument, we showed that $\dot{\gamma}_{v\to i} \sim \frac{\eta d_p}{m_p}\frac{1}{\mathscr{F}(\phi)^2}$.

The only difference between the scaling of Bagnold[12] and Degiuli et al.,[23] is in the choice of $\frac{1}{\lambda^2}$ or $\frac{1}{\mathscr{F}(\phi)^2}$. The difference between $\mathscr{F}(\phi)$ and λ can be seen in FIG. 5. The values of $\mathscr{F}(\phi)$ are our experimental estimate from the previous work[59]. It is noteworthy to mention that Bagnold's assumption in defining shear velocity fluctuations is based on the fact that the particles do not deform and consequently, the local shear rates enhance in the suspension in accordance to the relative values of particle size and surface to surface separation. Therefore, a naive enhancement

FIG. 5: (a) The ratio of the mean local shear rate to the average shear rate in the suspensions: (red line) $\dot{\gamma}_{local}/\dot{\gamma} = \lambda$ proposed by Bagnold[12], (black line) $\dot{\gamma}_{local}/\dot{\gamma} = \mathscr{F}(\phi)$, an experimental estimate from the measurements of the pressure imposed rheometry by Dagois-Bohy et al[59] (b) Plot of the ratio of λ to $\mathscr{F}(\phi)$ to show the difference between the estimates of Bagnold[12] and Dagois-Bohy et al[59] for the values of the mean local shear rate.

of the local shear rate, for a pure shearing motion can be given by Bagnold's estimate, i.e., $\dot{\gamma}_{local} = \dot{\gamma}\lambda$. However, recent works[23,42,59,62] have shown that the local shear rate is mainly controlled by the dynamics of particles which mainly depends on the geometrical constraints in the dense regime of suspensions. Therefore, the local shear rate is related to the average shear rate in the suspension via a geometric function $\dot{\gamma}_{local} = \dot{\gamma}\mathscr{F}(\phi)$. This geometric function $\mathscr{F}(\phi)$ has been measured theoretically, computationally[23,42]and experimentally[59].

In summary, following the scaling argument based on momentum exchange or energy conservation gives the same result, i.e., $\dot{\gamma}_{v\to i} \to 0$ as $\phi \to \phi_m$. This conclusion is in line with our experimental measurements showing that the transition from the viscous to inertial regime occurs at $Re_p << 1$ as we approach ϕ_m (FIG. 3 (c) & (d)). There exists a discrepancy between our observation and the results from discrete element method simulations in dense suspensions[25,35]. These results show that the transition from the viscous to inertial regime occurs at $Re_p \sim 1$. However, apparently our observation (i.e., $\dot{\gamma}_{v\to i} \to 0$ as $\phi \to \phi_m$) is in agreement with the above scalings and hybrid methods, i.e., simulation and theory, of perturbation close to the jamming[16,23,37–42].

On the other hand, it seems to be a difference between our experimental data and the prediction of the scaling arguments about the dependency of $\dot{\gamma}_{v\to i}$ on the particle size. Both scaling laws show $\dot{\gamma}_{v\to i} \sim 1/d_p^2$. Therefore, we expect a decrease in the values of $\dot{\gamma}_{v\to i}$ by a factor 4 as we enlarge the size of our particles from $d_p = 41.5\ \mu m$ to $d_p = 82.5\ \mu m$. However, we have an increase of $\dot{\gamma}_{v\to i}$ by about a factor of 2. This is a significant difference between the scaling laws (i.e., the predictions of Degiuli et al.,[23] and Bagnold[12]) and our observation. Nevertheless, FIG. 3 (e) & (f) show the collapse of data (for all the volume fraction) for a given particle size when we plot the stress vs the local particle Reynolds number. This means that the effect of the volume fraction in $\dot{\gamma}_{local} = \mathscr{F}(\phi)\dot{\gamma}$ is properly taken into account. This validates the approaches based on the local shear rate and the estimate value of the mean local shear rate, i.e., $\dot{\gamma}_{local} = \mathscr{F}(\phi)\dot{\gamma}$[59]. It is also noteworthy to mention that a version of what we define in this work as the local particle Reynolds

number has been also defined by Bagnold in his work[12] and it is called the Bagnold number, $Ba = \rho_p \dot{\gamma} d_p^2 \lambda^{1/2} / \eta_f$ (in our present study $\rho_p = \rho_f$). Although, $(Re_p)_{local}$ and Ba are not exactly the same but they both include local shear rate at the particle scale.

Based on the above explanations and several discussions that we have had with other scientists in the field (see the acknowledgement), the following might be the physical underlying mechanism of this viscous to inertial transition at such small values of shear rate. Because our data is above the random loose packing and our experiments are performed at the constant solid volume fraction, ephemeral force chains might span the flow and form and break as the shearing proceeds. Perhaps, it is the breaking of these chains to release elastic energy that will enhance the velocity of the colliding spheres. Consequently, the particle Reynolds number based on a relative velocity that is proportional to the shear rate alone will underestimate the velocity of collisions (as FIG. 3 (c) & (d) show that transition from the viscous to inertial regime occurs at $Re_p << 1$). So, in this view, the function of volume fraction ($\dot{\gamma}_{local}(\phi)$) adjusts the velocity of collisions to include the contribution associated with the elasticity of the force chains. This physical hypothesis is left to be validated experimentally. However, if such a hypothesis is correct, it might also explain the failure of the scaling arguments with the particle size alone as the length scale of the force chain should be taken into account. Testing this hypothesis requires an extensive study and perhaps design of a different experimental system that we intend to pursue in the future. Therefore, the current experimental measurements can provide a basis for the refinement and improvement of the future experimental, computational and theoretical works as we approach the jamming.

To conclude, our experimental results show while the proposed scaling laws successfully predict the dependency of $\dot{\gamma}_{v\to i}$ on the solid volume fraction through using $\dot{\gamma}_{local} = \mathscr{F}(\phi)\dot{\gamma}$, they fail in predicting the relationship between $\dot{\gamma}_{v\to i}$ and the particle size. Therefore, we speculate there seems to be a need for another length scale. However, currently we have no experimental or computational proof.

D. Transient flows of dense suspensions

Here, we adopt the limiting constitutive laws proposed in section III A and solve a boundary value problem and compare to our experimental results. The objective is to show the proposed equation (1) can predict the flows of suspensions in a transient setting. We impose a constant stress on the vane tool and solve the one dimensional momentum equation across the gap, equation (4),

FIG. 6: Prediction of the transient flow by the constitutive law for $d_p = 41.5$, $\phi = 0.57$, $\dot{\gamma}_{v\to i} = 1.6$(shown as green lines); (a): stress, τ, Vs. shear rate, $\dot{\gamma}$; (b): average shear rate evolution ($\bar{\dot{\gamma}}$) with time for all the imposed torques; (c)-(f): average shear rate evolution with time individually presented for the data points depicted in (a) and a comparison with the constitutive law prediction. (c)& (d): Two typical data points in viscous regime. Black solid lines: experimental data; Blue solid lines: the prediction of the flow using equation 1. (e)& (f) Two typical data points with the steady state shear rate in the inertial regime. Black solid lines: experimental data; Red lines: the prediction using the equation 1, Blue lines: Case 1, when suspension behaves viscously; Gray solid lines: Case 2, when suspension behaves inertially.

to calculate the velocity field.

$$\rho \frac{\partial u}{\partial t} = \frac{1}{r^2}\frac{\partial}{\partial r}(r^2\tau) \tag{4}$$

Here, ρ is the density of suspension which is the same as solid and fluid phases and the azimuthal velocity is denoted by u and τ is given in the equation (1), where $\dot{\gamma} = \dot{\gamma}_{r\theta}$. For the initial condition, we adopt the initial velocity distribution of the form $C_1/r + C_2 r$ with $C_1 = u_{preshear} R_c^2 R_b/(R_c^2 - R_b^2)$ and $C_2 = -u_{preshear} R_b/(R_c^2 - R_b^2)$. The $u_{preshear}$ is the steady state velocity of the vane in the pre-shear step. We apply the inertially corrected stress as the boundary condition, see the Supplementary Material for details of inertial correction. We have performed such an analysis for all the data points shown in FIG. 2, and we obtained a very good agreement between our experimental results and the prediction of the 1D momentum equation (4) coupled with the constitutive law of equation (1).

FIG. 6 shows a typical example of our results for particle size of $d_p = 41.5\mu m$ and solid volume fraction $\phi = 0.57$. Our experimental measurements for the relationship between shear stress and shear rate are given in FIG. 5 where $\dot{\gamma}_{v\to i} = 1.6\ s^{-1}$. When imposing a constant stress, the rheometer measures the rotational velocity of the vane tool and reports the average shear rate over the gap, $\bar{\dot{\gamma}}$. See the Supplementary Material for more details about calibrating the vane tool and calculating the correct value of the average shear rate from the rotating speed of the vane. FIG. 6 (b) shows the evolution of the average shear rate by time for all the imposed stresses. As explained before, there exists two timescales, one is associated with the transient time scale of the flow and the other is associated with the shear induced migration of the particles, i.e., final rise in the average shear

rate.

FIG. 6 (c)-(f) show the transient evolution of $\bar{\dot{\gamma}}$ for four data points depicted in FIG. 6 (a). For those cases that the suspensions behave viscously during the transient time, $\mathscr{H}(\dot{\gamma}-\dot{\gamma}_{v\to i})$ is always zero. In these cases the steady state shear rate is always below the $\dot{\gamma}_{v\to i}$. We have solved the equation (4) and calculated $\bar{\dot{\gamma}}$. FIG. 5 (c) & (d) show that the calculated average shear rates (shown in the blue solid line) follow the average shear rate data collected from the rheometer (shown in the black solid line).

In FIG. 6 (e) and (f), the steady state shear rate is larger than the value of $\dot{\gamma}_{v\to i}$, meaning that the suspension transitions from viscous to inertial regime during the evolution. Again our experiments follow the prediction of our 1D model, equation (2). To elaborate more on this we have solved the equation (2) twice by fixing the values of 0 (case 1) and 1 (case 2) for $\mathscr{H}(\dot{\gamma}-\dot{\gamma}_{v\to i})$, which correspond to a viscous and inertial suspension, respectively. The results are shown in FIG. 6 (e)&(f) as blue and gray lines, respectively. We note that the suspension is initially viscous and the true solution (red line) follows the case 1 solution. When the shear rate exceeds the value of $\dot{\gamma}_{v\to i}$, the suspension behaves inertially and the true solution follows case 2. This is another indication that the system transitions from the viscous regime to inertial regime at a critical shear rate of $\dot{\gamma}_{v\to i}$. In this section we have shown that the proposed constitutive laws in the dense regime can give a good prediction of a dynamic suspension flow that transitions from viscous to inertial regime.

IV. SUMMARY

This work explores the viscous to inertial mode of shear thickening in dense non-Brownian suspensions. A model suspension is designed in which spherical and mono-sized particles are suspended within an interstitial density matched fluid. Moreover, the interparticle forces are measured via a recently developed atomic force microscopy techniques. The rheology of this suspension is characterized via developing a unique protocol using volume imposed rheometry. The results show that our system of study is in the frictionless regime. Therefore, collisional and viscous forces are responsible for the dissipation of energy and transportation of momentum within the suspension.

We provide an empirical constitutive law (i.e., relationship between shear stress and shear rate) close to jamming volume fraction and show that this law coupled with momentum equation predicts the dynamics of dense suspensions in a transient flow. The simplicity of the proposed model suspension in conjunction with accurate force microscopy measurements make it a unique experi-

mental system to study non-Brownian suspensions exhibiting shear thickening. In near future, we will address several other interesting features of these suspensions in transient and inertial flow settings. This comprehensive experimental study from microscopic force measurements to macroscopic rheological characterization provide a basis for the refinement and development of ongoing theoretical and computational works in dense suspensions.

V. SUPPLEMENTARY MATERIAL

The detailed description of model suspension and sample preparation, vane tool calibration, explanation of average shear rate as the output of the rheometer, inertial correction, finding the rheometer's moment of inertia, Taylor Couette instability criteria, steady state viscosity behavior and results' size dependency and confinement is provided in the Supplementary materials. Additionally, the full set of experimental steady state data that are shown in FIG. 3 is presented in Table S1 of the Supplementary Materials.

ACKNOWLEDGMENTS

This work was supported by the National Science Foundation (grant CBET-1554044-CAREER) and OHIO Baker Fund Awards and in part by the National Science Foundation under Grant No. NSF PHY-1748958. We thank professor James T. Jenkins for fruitful discussions. We also acknowledge the Kavli Institute for Theoretical Physics (KITP) for hospitality during the course of this research. We thank professor Peter Olmsted for organizing the meeting entitled "Heterogeneous dynamics of confined dense suspensions" at KITP. This work has benefited from constructive discussions with the participants of the meeting.

REFERENCES

[1]J. J. Stickel and R. L. Powell, "Fluid mechanics and rheology of dense suspensions," Annu. Rev. Fluid Mech. **37**, 129–149 (2005).

[2]J. F. Morris, "A review of microstructure in concentrated suspensions and its implications for rheology and bulk flow," Rheologica acta **48**, 909–923 (2009).

[3]R. Mari, R. Seto, J. F. Morris, and M. M. Denn, "Shear thickening, frictionless and frictional rheologies in non-brownian suspensions," Journal of Rheology **58**, 1693–1724 (2014).

[4]Y. Madraki, S. Hormozi, G. Ovarlez, E. Guazzelli, and O. Pouliquen, "Enhancing shear thickening," Physical Review Fluids **2**, 033301 (2017).

[5]Y. Madraki, G. Ovarlez, and S. Hormozi, "Transition from continuous to discontinuous shear thickening: An excluded-volume effect," Physical review letters **121**, 108001 (2018).

[6]P. Sehgal, M. Ramaswamy, I. Cohen, and B. J. Kirby, "Using acoustic perturbations to dynamically tune shear thickening in colloidal suspensions," Phys. Rev. Lett. **123**, 128001 (2019).

[7]N. Y. Lin, C. Ness, M. E. Cates, J. Sun, and I. Cohen, "Tunable shear thickening in suspensions," Proceedings of the National Academy of Sciences **113**, 10774–10778 (2016).

[8]N. J. Wagner and J. F. Brady, "Shear thickening in colloidal dispersions," Physics Today **62**, 27–32 (2009).

[9]E. S. Yoo, J. H. Kim, W. Y. Jeong, H. K. Lee, J. K. Lee, J. T. Jun, N. H. Kwon, M. Y. Kwon, and D. Y. Lim, "Shear thickening fluid containing carbon nanoparticles and shock absorbing material comprising same," (2018), uS Patent 9,909,018.

[10]S. Gürgen, M. C. Kuşhan, and W. Li, "Shear thickening fluids in protective applications: a review," Progress in Polymer Science **75**, 48–72 (2017).

[11]R. Egres Jr, M. Decker, C. Halbach, Y. Lee, J. Kirkwood, K. Kirkwood, N. Wagner, and E. Wetzel, "Stab resistance of shear thickening fluid (stf)–kevlar composites for body armor applications," in *Transformational Science And Technology For The Current And Future Force: (With CD-ROM)* (World Scientific, 2006) pp. 264–271.

[12]R. A. Bagnold, "Experiments on a gravity-free dispersion of large solid spheres in a newtonian fluid under shear," Proceedings of the Royal Society of London. Series A. Mathematical and Physical Sciences **225**, 49–63 (1954).

[13]J. F. Brady and G. Bossis, "Stokesian dynamics," Annual review of fluid mechanics **20**, 111–157 (1988).

[14]R. Farr, J. R. Melrose, and R. Ball, "Kinetic theory of jamming in hard-sphere startup flows," Physical Review E **55**, 7203 (1997).

[15]N. Fernandez, R. Mani, D. Rinaldi, D. Kadau, M. Mosquet, H. Lombois-Burger, J. Cayer-Barrioz, H. J. Herrmann, N. D. Spencer, and L. Isa, "Microscopic mechanism for shear thickening of non-brownian suspensions," Physical review letters **111**, 108301 (2013).

[16]M. Wyart and M. Cates, "Discontinuous shear thickening without inertia in dense non-brownian suspensions," Physical review letters **112**, 098302 (2014).

[17]R. Seto, R. Mari, J. F. Morris, and M. M. Denn, "Discontinuous shear thickening of frictional hard-sphere suspensions," Physical review letters **111**, 218301 (2013).

[18]B. Guy, M. Hermes, and W. C. Poon, "Towards a unified description of the rheology of hard-particle suspensions," Physical review letters **115**, 088304 (2015).

[19]N. Y. Lin, B. M. Guy, M. Hermes, C. Ness, J. Sun, W. C. Poon, and I. Cohen, "Hydrodynamic and contact contributions to continuous shear thickening in colloidal suspensions," Physical review letters **115**, 228304 (2015).

[20]M. Hermes, B. M. Guy, W. C. Poon, G. Poy, M. E. Cates, and M. Wyart, "Unsteady flow and particle migration in dense, non-brownian suspensions," Journal of Rheology **60**, 905–916 (2016).

[21]J. Comtet, G. Chatté, A. Niguès, L. Bocquet, A. Siria, and A. Colin, "Pairwise frictional profile between particles determines discontinuous shear thickening transition in non-colloidal suspensions," Nature communications **8**, 15633 (2017).

[22]A. Fall, A. Lemaitre, F. Bertrand, D. Bonn, and G. Ovarlez, "Shear thickening and migration in granular suspensions," Physical review letters **105**, 268303 (2010).

[23]E. DeGiuli, G. Düring, E. Lerner, and M. Wyart, "Unified theory of inertial granular flows and non-brownian suspensions," Physical Review E **91**, 062206 (2015).

[24]A. Lemaître, J.-N. Roux, and F. Chevoir, "What do dry granular flows tell us about dense non-brownian suspension rheology?" Rheologica acta **48**, 925–942 (2009).

[25]M. Trulsson, B. Andreotti, and P. Claudin, "Transition from the viscous to inertial regime in dense suspensions," Physical review letters **109**, 118305 (2012).

[26]T. Kawasaki, A. Ikeda, and L. Berthier, "Thinning or thickening? multiple rheological regimes in dense suspensions of soft particles," EPL (Europhysics Letters) **107**, 28009 (2014).

[27]B. Andreotti, Y. Forterre, and O. Pouliquen, *Granular media: between fluid and solid* (Cambridge University Press, 2013).

[28]L. Amarsid, J.-Y. Delenne, P. Mutabaruka, Y. Monerie, F. Perales, and F. Radjai, "Viscoinertial regime of immersed granular flows," Physical Review E **96**, 012901 (2017).

[29]E. Koos, E. Linares-Guerrero, M. L. Hunt, and C. E. Brennen, "Rheological measurements of large particles in high shear rate flows," Physics of Fluids **24**, 013302 (2012).

[30]E. Linares-Guerrero, M. L. Hunt, and R. Zenit, "Effects of inertia and turbulence on rheological measurements of neutrally buoyant suspensions," Journal of Fluid Mechanics **811**, 525–543 (2017).

[31]S. Hormozi and I. Frigaard, "Dispersion of solids in fracturing flows of yield stress fluids," Journal of Fluid Mechanics **830**, 93–137 (2017).

[32]F. Boyer, É. Guazzelli, and O. Pouliquen, "Unifying suspension and granular rheology," Physical Review Letters **107**, 188301 (2011).

[33]C. Cassar, M. Nicolas, and O. Pouliquen, "Submarine granular flows down inclined planes," Physics of fluids **17**, 103301 (2005).

[34]C. Ness and J. Sun, "Flow regime transitions in dense non-brownian suspensions: Rheology, microstructural characterization, and constitutive modeling," Physical Review E **91**, 012201 (2015).

[35]C. Ness and J. Sun, "Shear thickening regimes of dense non-brownian suspensions," Soft Matter **12**, 914–924 (2016).

[36]S. Chialvo, J. Sun, and S. Sundaresan, "Bridging the rheology of granular flows in three regimes," Physical review E **85**, 021305 (2012).

[37]E. Lerner, G. Düring, and M. Wyart, "A unified framework for non-brownian suspension flows and soft amorphous solids," Proceedings of the National Academy of Sciences **109**, 4798–4803 (2012).

[38]E. Degiuli, E. Lerner, and M. Wyart, "Theory of the jamming transition at finite temperature," The Journal of chemical physics **142**, 164503 (2015).

[39]E. DeGiuli, J. McElwaine, and M. Wyart, "Phase diagram for inertial granular flows," Physical Review E **94**, 012904 (2016).

[40]G. Düring, E. Lerner, and M. Wyart, "Effect of particle collisions in dense suspension flows," Physical Review E **94**, 022601 (2016).

[41]E. DeGiuli and M. Wyart, "Unifying suspension and granular flows near jamming," in *EPJ Web of Conferences*, Vol. 140 (EDP Sciences, 2017) p. 01003.

[42]M. Trulsson, E. DeGiuli, and M. Wyart, "Effect of friction on dense suspension flows of hard particles," Physical Review E **95**, 012605 (2017).

[43]M. Rahmani, A. Hammouti, and A. Wachs, "Momentum balance and stresses in a suspension of spherical particles in a plane couette flow," Physics of Fluids **30**, 043301 (2018).

[44]P. M. Kulkarni and J. F. Morris, "Suspension properties at finite reynolds number from simulated shear flow," Physics of Fluids **20**, 040602 (2008).

[45]F. Picano, W.-P. Breugem, D. Mitra, and L. Brandt, "Shear thickening in non-brownian suspensions: an excluded volume effect," Physical review letters **111**, 098302 (2013).

[46]K. Yeo and M. R. Maxey, "Dynamics and rheology of concentrated, finite-reynolds-number suspensions in a homogeneous shear flow," Physics of Fluids **25**, 053303 (2013).

[47]D. Alghalibi, I. Lashgari, L. Brandt, and S. Hormozi, "Interface-resolved simulations of particle suspensions in newtonian, shear thinning and shear thickening carrier fluids," Journal of Fluid Mechanics **852**, 329–357 (2018).

[48]I. Lashgari, F. Picano, W.-P. Breugem, and L. Brandt, "Laminar, turbulent, and inertial shear-thickening regimes in channel flow of neutrally buoyant particle suspensions," Physical review letters **113**, 254502 (2014).

[49]F. Picano, W.-P. Breugem, and L. Brandt, "Turbulent channel flow of dense suspensions of neutrally buoyant spheres," Journal of Fluid Mechanics **764**, 463–487 (2015).

[50]W. Fornari, F. Picano, and L. Brandt, "Sedimentation of finite-size spheres in quiescent and turbulent environments," Journal of Fluid Mechanics **788**, 640–669 (2016).

[51]A. Prosperetti, "Life and death by boundary conditions," Journal of fluid mechanics **768**, 1–4 (2015).

[52]M. Gholami, A. Rashedi, N. Lenoir, D. Hautemayou, G. Ovarlez, and S. Hormozi, "Time-resolved 2d concentration maps in flowing suspensions using x-ray," Journal of Rheology **62**, 955–974 (2018).

[53]F. Peters, G. Ghigliotti, S. Gallier, F. Blanc, E. Lemaire, and L. Lobry, "Rheology of non-brownian suspensions of rough frictional particles under shear reversal: a numerical study," Journal of rheology **60**, 715–732 (2016).

[54]M. Sarabian, M. Firouznia, B. Metzger, and S. Hormozi, "Fully developed and transient concentration profiles of particulate suspensions sheared in a cylindrical couette cell," Journal of Fluid Mechanics **862**, 659–671 (2019).

[55]E. Azéma, N. Estrada, I. Preechawuttipong, J.-Y. Delenne, and F. Radjai, "Systematic description of the effect of particle shape on the strength properties of granular media," in *EPJ Web of Conferences*, Vol. 140 (EDP Sciences, 2017) p. 06026.

[56]B. Cambou, M. Jean, and F. Radjai, "Matériaux granulaires-modélisation et simulation numérique," (2012).

[57]N. Estrada, E. Azéma, F. Radjai, and A. Taboada, "Identification of rolling resistance as a shape parameter in sheared granular media," Physical Review E **84**, 011306 (2011).

[58]E. Azéma and F. Radjai, "Internal structure of inertial granular flows," Physical review letters **112**, 078001 (2014).

[59]S. Dagois-Bohy, S. Hormozi, É. Guazzelli, and O. Pouliquen, "Rheology of dense suspensions of non-colloidal spheres in yield-stress fluids," Journal of Fluid Mechanics **776** (2015).

[60]X. Chateau, G. Ovarlez, and K. L. Trung, "Homogenization approach to the behavior of suspensions of noncolloidal particles in yield stress fluids," Journal of Rheology **52**, 489–506 (2008).

[61]R. J. Flatt and P. Bowen, "Yodel: a yield stress model for suspensions," Journal of the American Ceramic Society **89**, 1244–1256 (2006).

[62]É. Guazzelli and O. Pouliquen, "Rheology of dense granular suspensions," Journal of Fluid Mechanics **852** (2018).

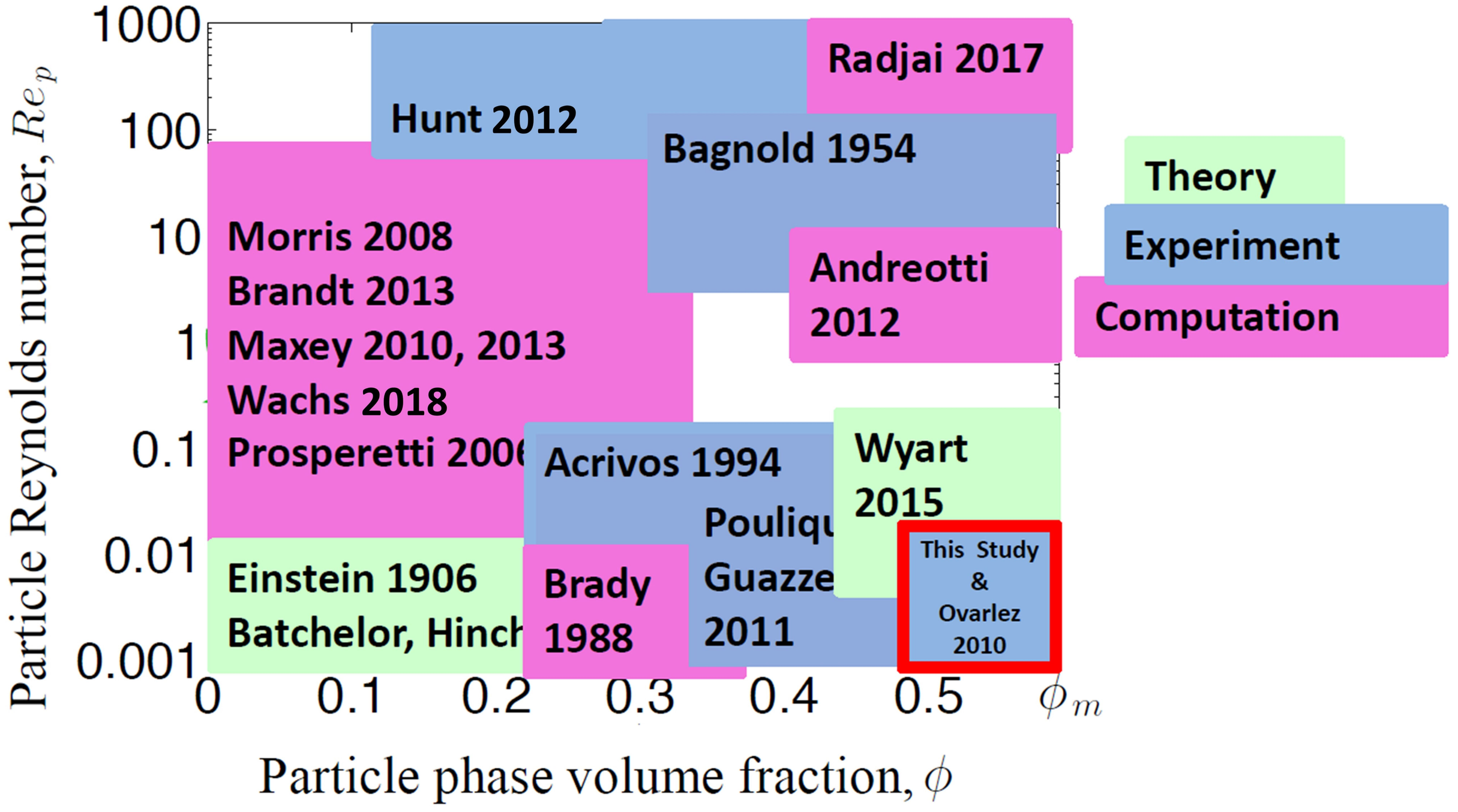

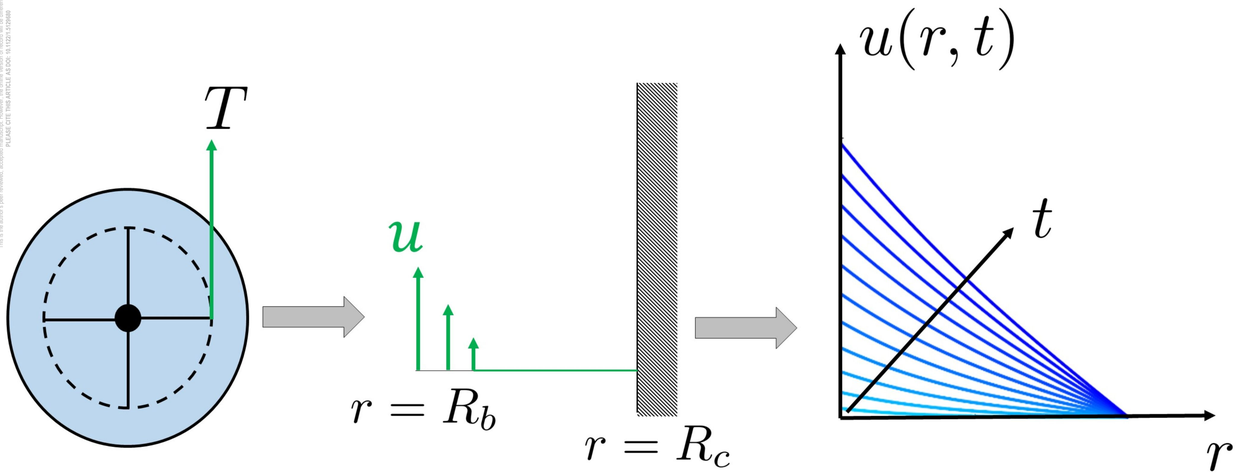

(a)

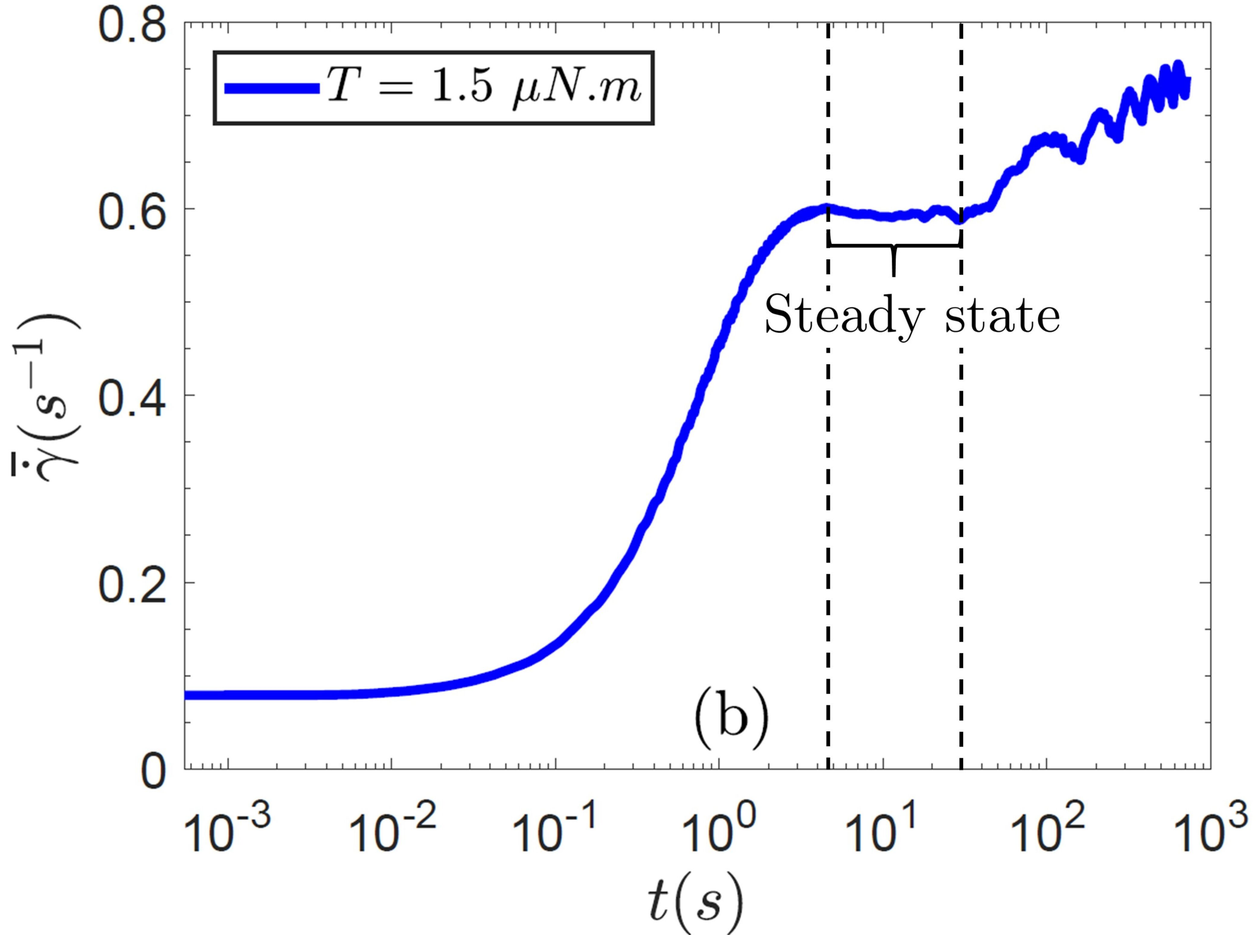

(b)